Systematic study of the dynamics about and between the Libration Points of the Sun-Earth-Moon System

Bastien Le Bihan, Josep Masdemont, Gérard Gómez, Stéphanie Lizy-Destrez

Systematic Study of the Dynamics about and between the Libration Points of the Sun-Earth-Moon System

By Bastien LE BIHAN,[1)] Josep J. MASDEMONT,[2)] Gerard GÓMEZ,[3)] and Stéphanie LIZY-DESTREZ[1)]

[1)]*ISAE-Supaéro, Toulouse, France*

[2)]*IEEC & Departament de Matemàtiques, Universitat Politècnica de Catalunya, Barcelona, Spain*

[3)]*IEEC & Departament de Matemàtiques i Informàtica, Universitat de Barcelona, Barcelona, Spain*

(Received June 21st, 2017)

A new approach is proposed for the systematic detection and refinement of natural connections between the libration points $\text{EML}_{1,2}$ of the Earth-Moon system and $\text{SEML}_{1,2}$ of the Sun-(Earth+Moon) system. It is structured around the Quasi-Bicircular Problem, a restricted coherent and periodic four-body dynamical model of the Sun-Earth-Moon system. The dynamics about the libration points are described by high-order periodic semi-analytical expansions obtained via the parameterization method. In their domain of convergence, such objects directly provide initial conditions at the departure point. They also allow to estimate the distance between any trajectory and the set of staging orbits (center manifold) at the targeted point. The potential connections can then be located and refined in the parameterization space. The transfer trajectories are finally successfully transposed in a higher-fidelity model based on JPL ephemerides.

Key Words: Sun-Earth-Moon system, restricted four-body problem, libration point, invariant manifolds, natural transfers

Nomenclature

$\mathbf{z}^{\text{em}}$	:	state in NCEM coordinates
$\mathbf{z}^{\text{sem}}$	:	state in NCSEM coordinates
H^{em}	:	Hamiltonian in NCEM coordinates
H^{sem}	:	Hamiltonian in NCSEM coordinates
θ	:	phase of the Sun-Earth-Moon (SEM) system
T	:	period of the SEM system
ω_s	:	pulsation of the SEM system
m_e	:	mass of the Earth
m_m	:	mass of the Moon
m_s	:	mass of the Sun
μ	:	Earth-Moon mass parameter
γ	:	distance between a libration point and the smallest primary
$\mathbf{W}$	:	expansion of the center manifold
$\mathbf{W}_s$	:	expansion of the center-stable manifold
$\mathbf{W}_u$	:	expansion of the center-unstable manifold
$\mathbf{s}$	:	reduced coordinates
Subscripts		
0	:	initial
f	:	final

1. Introduction

In recent decades, the integration of three-body dynamics in mission analysis has broaden space players' horizons, adding new possibilities for nominal orbit design, and considerably lowering the overall cost of specific transfers. Famous applications include SOHO[15)] and DSCOVR[33)] at the Sun-(Earth+Moon) libration point L_1 (SEML_1), as well as Gaia[29)] at SEML_2. Moreover, several cislunar and translunar missions – such as ARTEMIS[13)] – benefited from the Earth-Moon three-body dynamics, in particular about the libration point L_1 (EML_1) and L_2 (EML_2).

These applications built upon a deeper understanding of simple models of restricted three-body motions, starting with the Circular Restricted Three-Body Problem[34)] (CRTBP). In the latter, invariant tori and their associated stable, unstable, and center manifolds play a pivotal role in the system dynamics. Typically, the periodic orbits (one-dimensional tori) and quasi-periodic orbits (two-dimensional tori) about the equilibrium points yield staging orbit options while their hyperbolic invariant manifold provide dynamical channels that can be used as first guesses for efficient transfer options in higher-fidelity models.[3)]

From such studies, more complex mission design has been envisioned by approximating the Sun-Earth-Moon (SEM) multi-body system as two coupled three-body systems, in what can be seen as an extension of the patched conic approximation to three-body dynamics.[26)] In this approach, the invariant manifolds of the Sun-(Earth+Moon) and Earth-Moon problems can be suitably combined to produce efficient transfers. This so-called *coupled* CRTBP *approximation* paved the way for other combinations of invariant manifolds, for instance in the jovian system.[17,18)] Since then, the coupled approximation has been also used to perform Earth-to-EML_2[31,37)] and $\text{SEML}_{1,2}$-to-EML_2 transfers.[7,22)] All these applications uncovered a *low-energy network* that interconnects the Moon, the $\text{EML}_{1,2}$ and $\text{SEML}_{1,2}$ points, and the Earth (see Figure 1 for a simplified representation). This network is articulated around the natural interfaces between the libration regions of $\text{SEML}_{1,2}$ and $\text{EML}_{1,2}$.[26)] Hence, a deeper and more comprehensive analysis of such connections may serve as a foundation for the understanding and practical use of the network dynamics.

In that perspective, this paper intends to provide a systematic tool for the detection and refinement of $\text{SEML}_{1,2}$-$\text{EML}_{1,2}$ connections. It is mainly focused on the SEML_2-EML_2 case, but the fundamental concepts are easily adaptable to the other instances.

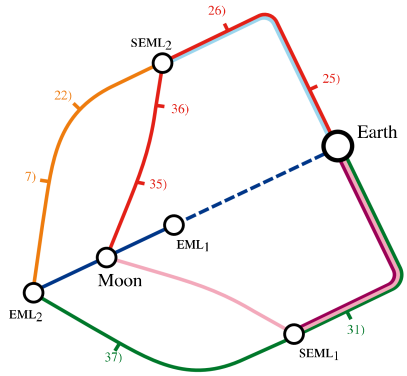

Fig. 1.: A representation of the Sun-Earth-Moon low-energy network. On each branch, a non-exhaustive list references that address the associated transfer problem are displayed.

Contrary to previous efforts based on the patched CRTBP approach, this tool is structured around a single dynamical model called the Quasi-Bicircular Problem (QBCP), which is a coherent periodic four-body model of the SEM system.[1)] Using the QBCP, a compact description of the dynamics about each libration point is obtained in the form of high-order, periodic, semi-analytical parameterizations of its invariant manifolds (center, center-stable and center-unstable). A brief analysis of the dynamics in the QBCP is presented in Section **2.**, along with key results on the form and evaluation of the semi-analytical expansions. Usually, the latter objects are used – within their domain of convergence – to compute initial conditions, whether on staging orbits (center manifold) or low-energy transfer legs (center-stable and center-unstable manifolds).[30)] In this paper, it is shown that they can also be used to estimate the distance between any six-dimensional state and a given center manifold. Such feature considerably ease the search for connections, as detailed in Section **4.**. The results can be shaped into families of possible connections that in turn can be refined into actual transfers, taking again advantage of the semi-analytical description at both ends. Such refinement procedure is described in Section **5.**. Finally, the families are transposed into a multi-body model based on the JPL ephemerides, in Section **6.**. It is then shown that the overall structure of the families are preserved in their refined JPL counterparts. This is a first step towards an *a posteriori* validation of the whole tool as a connection detector in higher-fidelity models.

2. Modelling the Sun-Earth-Moon system

This sections aims to present the Quasi-Bicircular Problem as a dynamical model of the SEM system and how it affects the invariant structures of the underlying Earth-Moon and Sun-(Earth+Moon) CRTBPs.

2.1. The Quasi-Bicircular Problem (QBCP)

The QBCP is a restricted four-body problem in which the three massive bodies – the Earth (m_e), the Moon (m_m) and the Sun (m_s) – are revolving in a coherent *planar* quasi-bicircular motion, the fourth mass – the spacecraft – being small and not influencing the motion of the primaries. The result is a non-autonomous Hamiltonian system that can be alternatively seen as the Earth-Moon CRTBP periodically-perturbed by the Sun, or the Sun-Earth CRTBP perturbed by the Moon.

The equations of the QBCP can be expressed in synodical systems of reference focused on two of the three primaries. In the Earth-Moon case, the corresponding frame, denoted $\mathcal{R}_{\text{EM}}$, is a rotating pulsating frame centered at the Earth-Moon barycenter in such a way that the Earth and the Moon are located at fixed points. As in the CRTBP, the system is made nondimensional by the following choice of units: the unit of mass is taken to be $m_m + m_e$; the unit of length is chosen to be the time-dependent separation between the centers of the Earth and the Moon; the unit of time is chosen such that the orbital period of the Earth-Moon motion is 2π. A similar frame, denoted $\mathcal{R}_{\text{SEM}}$, can be defined from the Sun-(Earth+Moon) perspective, taking the Sun and the Earth-Moon center of masse B_{em} as primaries.

In this paper, however, the equations of the QBCP are expressed in systems of reference adapted to each libration point. Indeed, synodical frames centered on libration points are fairly standard and have already been used in the CRTBP context, in order to guarantee good numerical properties.[24,32)] Taking again the Earth-Moon example, these frames are defined from $\mathcal{R}_{\text{EM}}$, with the following characteristics: (i) they are centered at the associated libration point $\text{EML}_{1,2}$, i.e. the geometrical position of this point in the Earth-Moon CRTBP; (ii) the unit of distance is redefined as the distance γ between $\text{EML}_{1,2}$ and the Moon. They are denoted $\mathcal{R}^i_{\text{EM}}, i = 1, 2$, and may be referred to as Normalized-Centered Earth-Moon (NCEM) Reference Frames. Figure 2 presents an XY-view of the $\mathcal{R}_{\text{EM}}$, $\mathcal{R}^1_{\text{EM}}$, and $\mathcal{R}^2_{\text{EM}}$ frames.

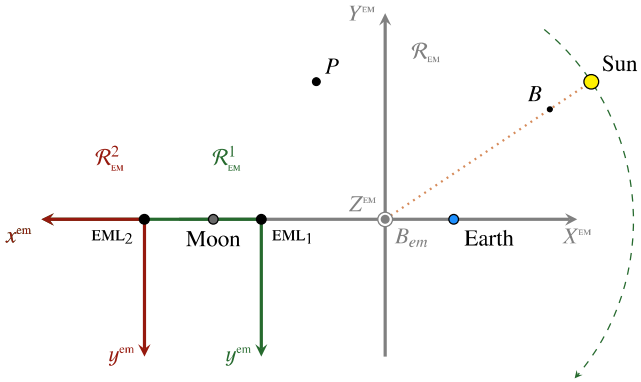

Fig. 2.: The Normalized-Centered Earth-Moon frames $\mathcal{R}^1_{\text{EM}}$ (in green) and $\mathcal{R}^2_{\text{EM}}$ (in red), along with the Earth-Moon Synodical frame $\mathcal{R}_{\text{EM}}$, viewed in the XY-plane.

Equivalent coordinates can be defined in the the case of $\text{SEML}_{1,2}$, and are denoted NCSEM coordinates.

2.2. Associated Hamiltonian

The NCEM case is addressed, the NCSEM case being formally equivalent. Let $\mathbf{z}^{\text{em}} = (\mathbf{x}^{\text{em}T}\ \mathbf{p}^{\text{em}T})^T = (x^{\text{em}}\ y^{\text{em}}\ z^{\text{em}}\ p_x^{\text{em}}\ p_y^{\text{em}}\ p_z^{\text{em}})^T$ be the position/momentum canonical state in NCEM coordinates. Moreover, let $C = \{e, m, s\}$ be the set of subscripts of the celestial bodies involved: the Earth (e), the Moon (m) and the Sun (s). For example, $\mathbf{x}_e^{\text{em}} = (x_e^{\text{em}}\ y_e^{\text{em}}\ z_e^{\text{em}})^T$ denotes the position vector of the Earth. The Hamiltonian of the QBCP in NCEM coordinates

takes the following form:

$$\begin{aligned} H^{\text{em}}(\mathbf{z}^{\text{em}},\theta) = \; & \frac{1}{2}\,\alpha_1(\theta)\left(p_x^{\text{em}\,2} + p_y^{\text{em}\,2} + p_z^{\text{em}\,2}\right) \\ & + \alpha_2(\theta)\left(p_x^{\text{em}}\,x^{\text{em}} + p_y^{\text{em}}\,y^{\text{em}} + p_z^{\text{em}}\,z^{\text{em}}\right) \\ & + \alpha_3(\theta)\left(p_x^{\text{em}}\,y^{\text{em}} - p_y^{\text{em}}\,x^{\text{em}}\right) - \alpha_9(\theta)x^{\text{em}} - \alpha_{10}(\theta)y^{\text{em}} \\ & - \frac{\alpha_6(\theta)}{\gamma^3}\sum_{c\in C}\frac{m_c}{\|\mathbf{x}^{\text{em}} - \mathbf{x}_c^{\text{em}}\|}, \end{aligned} \tag{1}$$

where m_c is the mass of the primary c. Moreover, the position vectors of the primaries are

$$\begin{aligned} \mathbf{x}_e^{\text{em}} &= \begin{pmatrix} \dfrac{-1\pm\gamma}{\gamma} & 0 & 0 \end{pmatrix}^T, \quad \mathbf{x}_m^{\text{em}} = \begin{pmatrix} \pm 1 & 0 & 0 \end{pmatrix}^T, \\ \mathbf{x}_s^{\text{em}}(\theta) &= \begin{pmatrix} \dfrac{\mu - 1 \pm \gamma - \alpha_7(\theta)}{\gamma} & -\dfrac{\alpha_8(\theta)}{\gamma} & 0 \end{pmatrix}^T, \end{aligned} \tag{2}$$

where μ is the Earth-Moon mass ratio, and where the upper (resp. lower) signs stands for the EML_1 (resp. EML_2) case. Finally, the functions $\alpha_k(\theta), k \in [\![1, 10]\!]$ are trigonometric functions of the form:

$$\begin{aligned} \alpha_k(\theta) &= \alpha_{k0} + \sum_{j\geqslant 1}\alpha_{kj}\cos(j\theta), \text{ for } k = 1,3,4,6,7,9 \\ \alpha_k(\theta) &= +\sum_{j\geqslant 1}\alpha_{kj}\sin(j\theta), \qquad \text{for } k = 2,5,8,10 \end{aligned}$$

where θ is the phase of the Sun-Earth-Moon system, used to parameterize the time-dependency of the dynamics. In NCEM coordinates, θ is the phase of the Sun with respect to the Earth-Moon line. The first α_{kj} coefficients are available in[1] (resp.[28]) in the EM (resp. SEM) case.

The angle θ is directly proportional to the time t: $\theta = \omega_s t$, where ω_s is the pulsation of the SEM system which, in NCEM coordinates, corresponds the pulsation of the Sun with respect to the Earth-Moon binary motion. The Hamiltonian H^{em} is 2π-periodic in θ and T-periodic in time, where $T = 2\pi/\omega_s$ is the period of the Sun-Earth-Moon system.

Finally, a similar Hamiltonian $H^{\text{sem}}(\mathbf{z}^{\text{sem}},\theta)$ can be derived from the Sun-(Earth+Moon) perspective, in NCSEM coordinates. Since all the qualitative results hold in both cases, the superscripts $^{\text{em}}$ and $^{\text{sem}}$ are discarded whenever the context is clear.

2.3. Corresponding equations of motion.

The equations of motion are immediately derived from the Hamiltonian, using the following relation:

$$\dot{\mathbf{z}} = \mathbf{f}(\mathbf{z},\theta) = \mathbf{J}\partial_{\mathbf{z}}H(\mathbf{z},\theta) = \mathbf{J}\frac{\partial H}{\partial \mathbf{z}}(\mathbf{z},\theta) \tag{3}$$

where $\mathbf{J}$ is the following symplectic matrix:

$$\mathbf{J} = \begin{pmatrix} \mathbf{0} & \mathbf{I}_3 \\ -\mathbf{I}_3 & \mathbf{0} \end{pmatrix}, \tag{4}$$

and $\mathbf{I}_3$ is the 3×3 identity matrix.

2.4. Dynamics about a libration point in the QBCP

In the QBCP, ought to the presence of a periodic perturbation, the libration points are no longer fixed points but are replaced by planar 2π-periodic orbits in the variable θ, referred to as the dynamical equivalents of the libration points.[8,14] Nevertheless, the perturbation is small enough to preserve the global structures of the dynamics inherited from the CRTBP.[2] Namely, the linearized motion about the libration orbits are still the products of two centers and one saddle, and we can again define a center, a center-stable, and a center-unstable manifolds, all these objects being carried over to the full nonlinear problem.

More explicitly, using Floquet theory of periodic systems, we can show that there exists a symplectic change of coordinates of the form

$$\mathbf{z}^{\text{em}} = \mathbf{P}(\theta)\mathbf{C}\hat{\mathbf{z}} + \mathbf{V}(\theta), \tag{5}$$

so that, in the new complex variable $\hat{\mathbf{z}} = (\hat{\mathbf{x}}^T \;\; \hat{\mathbf{p}}^T)^T = (\hat{x}\;\hat{y}\;\hat{z}\;\hat{p}_x\;\hat{p}_y\;\hat{p}_z)^T$, the Hamiltonian of the system takes the form

$$\hat{H}(\hat{\mathbf{z}},\theta) = i\omega_1\hat{x}\hat{p}_x + \omega_2\hat{y}\hat{p}_y + i\omega_3\hat{z}\hat{p}_z + \sum_{k=3}\hat{H}_k(\hat{\mathbf{z}},\theta) \tag{6}$$

where $\omega_i \in \mathbb{R}, i = 1,2,3$, and where $\hat{H}_k(\hat{\mathbf{z}},\theta)$ are homogeneous Fourier-Taylor polynomials, i.e. homogeneous polynomials of degree k in $\hat{\mathbf{z}}$, with Fourier series in the variable θ as coefficients. From Equation (6), one can see that the linearized motion is of type center $\times$ saddle $\times$ center, as in the CRTBP case.[19]

The derivation of the change of coordinates (5) has been performed in previous references – at least in the $\text{EML}_{2,3,4}$ case.[1,16] The reader is kindly referred to these articles for technical details. It is only briefly recalled that Equation (5) is the composition of three operations:

- A translation vector $\mathbf{V}(\theta)$, which is a 6×1, 2π-periodic, real vector of the form $\mathbf{V}(\theta) = (v_1\;v_2\;0\;v_4\;v_5\;0)^T$, where each coefficient $v_i(\theta)$ is a Fourier series in θ. It corresponds to the Fourier transform of the trajectory associated with the dynamical equivalents of the libration point. With this translation, the origin becomes a fixed point.
- A rotation matrix $\mathbf{P}(\theta)$, which is a 6×6, 2π-periodic, real matrix whose components $p_{ij}(\theta)$ are Fourier series in θ.
- Finally, $\mathbf{C}$ is a constant 6×6 complex matrix and corresponds to a complexification of the variables associated to the two centers.

Note that the variable $\hat{\mathbf{z}}$ and the Hamiltonian $\hat{H}$ are both complex, although the original dynamics are real. All the subsequent semi-analytical procedures are performed using the variable $\hat{\mathbf{z}}$, hence in complex form. However, it is always possible to go back to the real NC coordinates by applying Equation (5).

The linearization and the change of coordinates (5) showed that the motion about each libration point has the same structure as in the CRTBP, with an additional frequency. In particular, the center manifold – product of the two centers – is again a normally hyperbolic invariant manifold (NHIM), associated to a stable and an unstable manifolds. In a small neighborhood of the libration points, these results can be extended to the nonlinear dynamics since NHIMS persist under small perturbations.[11]

The next subsection presents a semi-analytical description of these time-dependent invariant manifolds about the libration points, obtained via the parameterization method.

3. The parameterization of invariant manifolds in the QBCP

This section introduces the form of the semi-analytical expansions of the invariant manifolds – the center, center-stable and center-unstable – about the libration points $\text{EML}_{1,2}$ and $\text{SEML}_{1,2}$ in the QBCP. Such description has been obtained via a custom extension of the parameterization method (PM)[5,21] to the invariant manifolds about periodically-perturbed equilibriums.[28] The sequel focuses only on results and does not provide any substantial description of the underlying semi-analytical algorithm. Please refer to[28] for details on the current implementation.

3.1. The case of the center manifold

Applying the parameterization method to the center manifold and the change of coordinates (5), it is possible to find a function

$$\begin{array}{rccc} \mathbf{W} & : & \mathbb{R}^4 \times \mathbb{R} & \rightarrow & \mathbb{R}^6 \\ & & (\mathbf{s}, \theta) & \mapsto & \mathbf{W}(\mathbf{s}, \theta), \end{array} \tag{7}$$

that parameterizes the center manifold in a given neighborhood about the origin, in NC coordinates. Moreover, using the *graph style*, a simple form can be obtained – see[21] for a detailed explanation of the possible styles of the parameterization method, and again[28] for the current implementation. Denoting $\mathbf{W} = (W_1\ W_2\ W_3\ W_4\ W_5\ W_6)^T$, the following equalities hold:

$$\begin{pmatrix} W_1 \\ W_2 \\ W_4 \\ W_5 \end{pmatrix} = \omega_1 \underbrace{\begin{pmatrix} p_{11} & -p_{14} \\ p_{21} & -p_{24} \\ p_{41} & -p_{44} \\ p_{51} & -p_{54} \end{pmatrix} \begin{pmatrix} s_3 \\ s_1 \end{pmatrix}}_{\text{order 1 in } \mathbf{s}} + \underbrace{\begin{pmatrix} p_{12} & p_{15} \\ p_{22} & p_{25} \\ p_{42} & p_{45} \\ p_{52} & p_{55} \end{pmatrix} \begin{pmatrix} \tilde{y}(\mathbf{s}, \theta) \\ \tilde{p}_y(\mathbf{s}, \theta) \end{pmatrix}}_{\text{order } k \geqslant 2}, \tag{8}$$

and, for the vertical motion:

$$\begin{pmatrix} W_3 \\ W_6 \end{pmatrix} = \omega_3 \begin{pmatrix} p_{33} & -p_{36} \\ p_{63} & -p_{66} \end{pmatrix} \begin{pmatrix} s_4 \\ s_2 \end{pmatrix}, \tag{9}$$

where the dependence in θ of the components p_{ij} of $\mathbf{P}$ has been omitted in both equations. Moreover, $\tilde{y}(\mathbf{s}, \theta)$ and $\tilde{p}_y(\mathbf{s}, \theta)$ are full Fourier-Taylor series of order (N, J), starting at order $k = 2$. More explicitly, taking the example of $\tilde{y}$:

$$\tilde{y}(\mathbf{s}, \theta) = \sum_{k=2}^{N} \tilde{y}_k^p(\hat{\mathbf{s}}, \theta) = \sum_{k=2}^{N} \sum_{\mathbf{r} \in \mathcal{R}^k} w_{\mathbf{r}}(\theta) \mathbf{s}^{\mathbf{r}}, \tag{10}$$

where $\mathcal{R}^k = \left\{ \mathbf{r} \in \mathbb{N}^4, |\mathbf{r}| = r_1 + \cdots + r_4 = k \right\}$, $\mathbf{s}^{\mathbf{r}} = s_1^{r_1} s_2^{r_2} s_3^{r_3} s_4^{r_4}$, and the coefficients $w_{\mathbf{r}}(\theta)$ are Fourier series of the form:

$$w_{\mathbf{r}}(\theta) = \sum_{j=-J}^{J} w_{\mathbf{r},j} e^{ij\theta}.$$

An equivalent form exists for $\tilde{p}_y(\mathbf{s}, \theta)$.

Practical use. The parameterization method is generically a divergent process, due to the crossing of resonances.[21] In particular, if we stop the expansion to a given order N, the remainder behaves like $O(R^{N+1})$, where R denotes the distance to the origin.[23] Hence, there exists a practical domain of convergence $\mathcal{D}_c$ about the origin that can be estimated numerically . Both the practical radius of convergence and the optimal value for N have been estimated *a posteriori*, using extended error testing campaigns about each libration point.[27,28] It has been found that $N = 20$ is a good compromise as a common order for the four center manifolds that have been studied, at $\text{EML}_{1,2}$ and $\text{SEML}_{1,2}$. Furthermore, each Fourier series $w_{\mathbf{r}}(\theta)$ is truncated to a certain order J ($j \leqslant J$), $J = 30$ being far enough to include any relevant term in practice.

Once N and J have been fixed, for any vector of reduced coordinates $\mathbf{s} = (s_1\ s_2\ s_3\ s_4)^T$ in $\mathcal{D}_c$, $\mathbf{z} = \mathbf{W}(\mathbf{s}, \theta)$ yields initial conditions in the center manifold, in NC coordinates. Note that the parameterization $\mathbf{W}$ takes into account the explicit and periodic time-dependency of the dynamics via the variable θ.

Planar motion. An immediate conclusion from Equation (9) is that the vertical motion is linear and depends only on the components s_2 and s_4. Hence, imposing $s_2 = s_4 = 0$ guarantees that the description of the manifolds – and more generally the dynamics – are enclosed in the xy-plane. However, whenever s_2 and s_4 are non null, they influence the dynamics in all directions, since these components appear in the expansions $\tilde{y}(\mathbf{s}, \theta)$ and $\tilde{p}_y(\mathbf{s}, \theta)$.

3.2. The projection method inside the center manifold

Given an NC state $\mathbf{z}(t)$ inside the center manifold, it is possible to find its reduced coordinates $\mathbf{s} \in \mathbb{R}^4$ so that $\mathbf{z}(t) = \mathbf{W}_s(\mathbf{s}, \omega_s t)$, as long as the graph style is used. In practice, given a time t and a state $\mathbf{z}(t)$ assumed inside the center manifold, $\mathbf{s}$ is obtained via the following inverse function:

$$\mathbf{s} = \mathbf{W}_s^{-1}(\mathbf{z}, t) = \mathbf{\Omega} \mathbf{P}^{-1}(\theta) \left[\mathbf{z}(t) - \mathbf{V}(\theta) \right], \tag{11}$$

where $\theta = \omega_s t$, and

$$\mathbf{\Omega} = \begin{pmatrix} 0 & 0 & 0 & -\frac{1}{\omega_1} & 0 & 0 \\ 0 & 0 & 0 & 0 & 0 & -\frac{1}{\omega_3} \\ \frac{1}{\omega_1} & 0 & 0 & 0 & 0 & 0 \\ 0 & 0 & \frac{1}{\omega_3} & 0 & 0 & 0 \end{pmatrix}.$$

Such inversion is possible providing that $\mathbf{P}(\theta)$ is invertible, which is always the case in practice.

3.3. The case of the center-(un)stable manifold

Using the parameterization method, it is also possible to compute the semi-analytical descriptions of the center-stable ($\mathbf{W}_s$) and center-unstable ($\mathbf{W}_u$) manifolds about each libration point.[21] Both cases yield very similar results that differ only by a few symmetries. In the case of the center-unstable manifold, the result of the PM is a vector of Fourier-Taylor series $\mathbf{W}_u(\mathbf{s}, \theta)$ of the form

$$\begin{array}{rccc} \mathbf{W}_u & : & \mathbb{R}^5 \times \mathbb{R} & \rightarrow & \mathbb{R}^6 \\ & & (\mathbf{s}, \theta) & \mapsto & \mathbf{W}_u(\mathbf{s}, \theta) \end{array} \tag{12}$$

The fifth component s_5 parameterizes the hyperbolic unstable direction. When $s_5 = 0$, the center manifold is retrieved. Moreover, the vertical components in $\mathbf{W}_u$ do not depend on s_5 and are actually equal to their center counterparts. In particular, the motion can still be made planar by imposing $s_2 = s_4 = 0$.

4. Finding EML_2-$\text{SEML}_{1,2}$ connections

We know from previous works – notably[6,10,37] – that there exist natural planar and three-dimensional connections between the center or center-hyperbolic manifolds about EML_2 and $\text{SEML}_{1,2}$. In this section, we are interested in producing ballistic transfers between the center-unstable manifold about EML_2

and the center-stable manifolds about SEML_1 and SEML_2, in a systematic fashion. The numerical tool developed to detect such connections is heavily based on the semi-analytical description presented in Section **3.**.

4.1. A Two-Point Boundary Value Problem

The problem of finding natural transfers between the center-unstable manifold about EML_2 and the center-stable manifolds about SEML_1 and SEML_2 falls into the category of *Two-Point Boundary Value Problems* (TPBVP). We denote $\mathcal{W}_u$ the center-unstable manifold about EML_2 and $\mathcal{W}_s$ the center-stable manifold about either SEML_1 or SEML_2. Moreover, we suppose that the state $\mathbf{z}$ is here given in NCSEM coordinates, and so is the vector field $\mathbf{f}(\mathbf{z}, t)$. In practice, the NCSEM coordinates have proven to be the ideal coordinate system for such problem. Indeed, in this framework, the unit of length is the distance between B_{em} and $\text{SEML}_{1,2}$, which roughly corresponds to the size of an EML_2-$\text{SEML}_{1,2}$ connection.

The problem of finding natural connections between $\mathcal{W}_u$ at time $t = t_0$ and $\mathcal{W}_s$ at time $t = t_f$ can be written as follows:

$$\dot{\mathbf{z}} = \mathbf{f}(\mathbf{z}, t), \qquad \mathbf{z}(t_0) \in \mathcal{W}_u, \qquad \mathbf{z}(t_f) \in \mathcal{W}_s, \tag{13}$$

where the vector field $\mathbf{f}$ is formally given in Equation (3).

The main difficulty here lies in the derivation of a closed form for the boundary conditions. This is where the semi-analytical expansions come into play. Within their respective domain of practical convergence, $\mathbf{W}_u(\mathbf{s}, \theta)$ and $\mathbf{W}_s(\mathbf{q}, \theta)$, the parameterizations of $\mathcal{W}_u$ and $\mathcal{W}_s$, can be used to explicitly parameterize the starting and arrival sets. Using this idea, the previous problem can be formulated again as follows:

$$\begin{aligned} \dot{\mathbf{z}} = \mathbf{f}(\mathbf{z}, t), \quad & \exists \mathbf{s}_0 \in \mathbb{R}^5,\ \mathbf{z}(t_0) = \boldsymbol{C}_e^s \circ \mathbf{W}_u(\mathbf{s}_0, \omega_s t_0), \\ & \exists \mathbf{q}_f \in \mathbb{R}^5,\ \mathbf{z}(t_f) = \mathbf{W}_s(\mathbf{q}_f, \omega_s t_f), \end{aligned} \tag{14}$$

where $\boldsymbol{C}_e^s$ is the change of coordinates between the NCEM and NCSEM frameworks. Denoting $\mathbf{z}^{\text{em}}$ the state in NCEM coordinates, the function $\boldsymbol{C}_e^s(\mathbf{z}^{\text{em}})$ takes the form:

$$\boldsymbol{C}_e^s(\mathbf{z}^{\text{em}}) = \mathbf{R}_e^s(\theta)\, \mathbf{z}^{\text{em}} + \mathbf{B}_e^s(\theta), \tag{15}$$

where $\mathbf{R}_e^s(\theta)$ is a $6, \times 6$ 2π-periodic matrix, and $\mathbf{B}_e^s(\theta)$ is a 6×1, 2π-periodic vector that are not explicitly given here.

In the TPBVP (14), the adjustment variables are not $\mathbf{z}(t_0)$ and $\mathbf{z}(t_f)$ anymore but their reduced counterparts, i.e. $\mathbf{s}_0$ and $\mathbf{q}_f$. Note that we have favored the notation $\mathbf{q}_f$ instead of $\mathbf{s}_f$ for the reduced coordinates at $\text{SEML}_{1,2}$, essentially to avoid any confusion between the invariant manifolds at EML_2 and $\text{SEML}_{1,2}$.

Although appealing, this formulation does not impose any constraint on the initial state $\mathbf{s}_0$ nor the targeted state $\mathbf{q}_f$, for which it could be very difficult to formulate a first guess. To address this problem, a rough grid search is performed on the initial state $\mathbf{s}_0$, coupled with a projection method, based on the results of Section **3.2.**, and detailed hereafter.

4.2. The projection-based research procedure

Written in the following generic form, the procedure is perfectly applicable to three-dimensional connections, although we will focus on the planar problem on the numerical applications.

First, the initial time t_0 is fixed to a given value in $[0, T]$, which corresponds to a certain phase $\theta_0 = \omega_s t_0$ of the Sun-Earth-Moon system. Since we are looking for natural transfers, it is necessary to start along the unstable direction at EML_2, and therefore s_5 must be non null in $\mathbf{s}_0$. However, there is no need to make it a free variable since it does not parameterize the motion inside the center manifold. For this reason, the unstable component is set to a fixed small value $s_5 = \epsilon$.

Then, a discrete set $\mathcal{F}_c$ of initial conditions $\mathbf{s}_0$ is taken inside the domain of practical convergence of $\mathbf{W}_u(\mathbf{s}, \theta)$ at EML_2. In practice, in the planar case, this corresponds to initial conditions of the form $\mathbf{s}_0 = (s_1, 0, s_3, 0, \epsilon)^T$, with $(s_1, s_3) \in [-35, 35]^2$.

For all initial conditions $(\mathbf{s}_0 \in \mathcal{F}_c, t_0)$, the initial state $\mathbf{z}_0 = \boldsymbol{C}_e^s \circ \mathbf{W}_u(\mathbf{s}_0, \theta_0)$ is evaluated and numerically integrated on an arbitrarily long time span $[t_0, t_f]$. The result of each integration is stored on a time grid $\mathcal{T}_c = [t_0, t_1, \ldots, t_{n-1}, t_n = t_f]$, with $n \in \mathbb{N}$. We denote $\mathbf{z}_j(\mathbf{s}_0, t_0)$ the resulting state at time t_j, $j \in [\![1, n]\!]$.

Each state $\mathbf{z}_j(\mathbf{s}_0, t_0)$ is *projected* on the center manifold $\mathcal{W}_c$ at $\text{SEML}_{1,2}$, using the following procedure: if we assume that $\mathbf{z}(t) \in \mathcal{W}_c$ and is close enough to the libration point, then there exists a reduced state $\mathbf{q}_p \in \mathcal{D}_c \subset \mathbb{R}^4$ such that $\mathbf{z}(t) = \mathbf{W}_c(\mathbf{q}_p, \omega_s t)$, where $\mathbf{W}_c$ is the parameterization of $\mathcal{W}_c$ and $\mathcal{D}_c$ is its domain of practical convergence. An estimate of $\mathbf{q}_p$ can then be directly computed by using Equation (11). It can be checked *a posteriori* that $\mathbf{q}_p$ is in fact inside $\mathcal{D}_c$. We assume that it is the case in the sequel.

Let apply again $\mathbf{W}_c$ and define $\mathbf{z}_p(t) := \mathbf{W}_c(\mathbf{q}_p, \omega_s t)$. Of course, in practice, $\mathbf{z} \notin \mathcal{W}_c$ and $\mathbf{z}_p$ is different from $\mathbf{z}$, and $\mathbf{z}_p$ is denoted the *projection* of $\mathbf{z}$ on $\mathcal{W}_c$. We can evaluate the discrepancy between $\mathbf{z}_0$ and $\mathbf{z}_p$, using the distance $d_p(\mathbf{z}, t)$ defined by

$$d_p(\mathbf{z}, t) := \|\mathbf{z} - \mathbf{z}_p(t)\| = \left\|\mathbf{z} - \mathbf{W}_c(\mathbf{q}_p, \omega_s t)\right\|. \tag{16}$$

The function $d_p(\mathbf{z}, t)$ provides a measure of the distance to the center manifold: the closer $\mathbf{z}$ to $\mathbf{W}_c$ at time t, the smaller $d_p(\mathbf{z}, t)$. Note that, once the parameterization $\mathbf{W}_c$ has been fixed, d_p only depends on the current state $\mathbf{z}$ and the time t.

For any initial condition $(\mathbf{s}_0 \in \mathcal{F}_c, t_0)$, the projection distance $d_p(\mathbf{z}_j, t_j)$ can be computed for all $j \in [\![1, n]\!]$ and the minimum among these values can be selected:

$$d_p^m(\mathbf{s}_0, t_0) = \min_{j \in [\![1,n]\!]} d_p(\mathbf{z}_j, t_j). \tag{17}$$

Denoting $j_m = \underset{j \in [\![1,n]\!]}{\operatorname{argmin}}\, d_p(\mathbf{z}_j, t_j)$, the projection $\mathbf{q}_p^m$ that is associated with this minimum is given by

$$\mathbf{q}_p^m(\mathbf{s}_0, t_0) = \mathbf{W}_c^{-1}(\mathbf{z}_{j_m}, t_{j_m}). \tag{18}$$

Note that, since all $\mathbf{z}_j$ are functions of $(\mathbf{s}_0, t_0)$, the minimum distance d_p^m and the associated projection $\mathbf{q}_p^m$ only depend on $(\mathbf{s}_0, t_0)$, providing that the time grid $\mathcal{T}_c$ has been fixed.

The minimum distance $d_p^m(\mathbf{s}_0, t_0)$ can be computed for all initial conditions $(\mathbf{s}_0 \in \mathcal{F}_c, t_0)$. If there exist a value of $\mathbf{s}_0$ for which d_p^m is small enough – in practice, below a given threshold – we can consider that we have found a good estimate of a solution for the TPBVP (14), with

$$\begin{aligned} \mathbf{q}_f &= \begin{pmatrix} \mathbf{q}_p^m \\ 0 \end{pmatrix}, \\ t_f &= t_{j_m}, \end{aligned} \tag{19}$$

i.e. the hyperbolic component q_5 approximated by zero. A schematic illustration of the projection procedure up to Equation (16) is given on Figure 3.

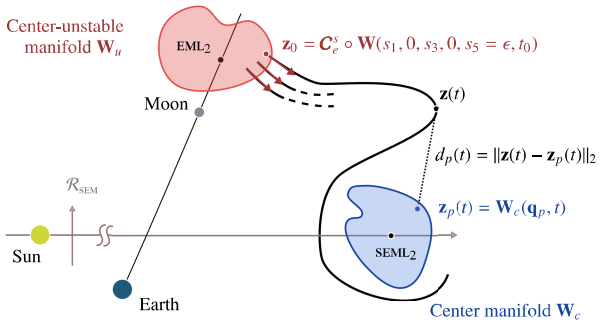

Fig. 3.: Schematic illustration of the projection-based research procedure. See text for details, in particular for the definition of the vector $\mathbf{q}_p$.

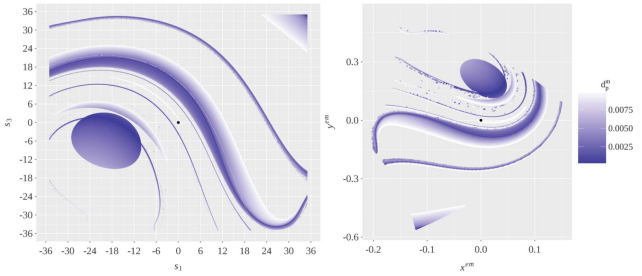

(a) As a function of (s_1, s_3). (b) As a function of $(x^{\text{em}}, y^{\text{em}})$.

Fig. 4.: The minimum distance of projection d_p^m for $t_0 = 0.99T$, where T is the period of the Sun-Earth-Moon system. Only the points for which $d_p^m < 10^{-2}$ are plotted. The symbol ● locates EML$_2$ on the two plots.

4.3. Example of planar results

The planar condition can be ensured simply by imposing $s_2 = s_4 = 0$ in all initial conditions $(\mathbf{s}_0 \in \mathcal{F}_c, t_0)$. Therefore, for a fixed initial time t_0, the minimum distance $d_p^m(\mathbf{s}_0, t_0)$ only depends on two variables, namely (s_1, s_3).

Figure 4a provides an example of the map $(s_1, s_3) \mapsto d_p^m(s_1, s_3, t_0)$ in the case of an EML$_2$-SEML$_2$ transfer, and for $t_0 = 0.99T$ (arbitrary choice). Figure 4b displays the same results as a function of $(x^{\text{em}}, y^{\text{em}})$, in NCEM coordinates. What we see appear are blue "valleys" of solutions of the TPBVP, corresponding to small values of $d_p^m(s_1, s_3, t_0)$. The same structures are visible on both plots.

Since the initial time has been fixed to $t_0 = 0.99T$, Figure 4 represents a snapshot of all the (relatively) good initial conditions that produce planar EML$_2$-SEML$_2$ connections. However, we are naturally limited by the scope of the domains of practical convergence at both ends. This domain is directly visible for EML$_2$, it corresponds to the size of the cartesian box displayed on Figure 4a. The domain $\mathcal{D}_c$ about SEML$_2$ is also partially visible: indeed, the procedure previously described includes a check on whether the projection $\mathbf{q}_p^m$ is found in $\mathcal{D}_c$. If it is not the case, the corresponding distance d_p^m is considered virtually infinite and is not displayed on the maps, which can create numerical artifacts. For instance, the clean round shape visible on both plots corresponds to the boundaries of $\mathcal{D}_c$ around SEML$_2$ as seen from this particular region about EML$_2$.

Equivalent maps can be produced for any initial time $t_0 \in [0, T]$, hence providing a complete overview of the families of approximated *planar* connections from the EML$_2$ point of view. However, the precision with which such solutions are obtained greatly depends on the resolution of the discretized set $\mathcal{F}_c$ at EML$_2$. Moreover, such maps provide little information on the targeted orbits at SEML$_{1,2}$. In order to tackle both issues, a refinement process based on a multiple shooting scheme has been implemented, as described hereafter.

5. Refinement of EML$_2$-SEML$_{1,2}$ connections

5.1. The multiple shooting procedure

Given an initial guess $(\mathbf{s}_0, t_0, \mathbf{q}_f, t_f)$ from the projection method, the idea is to use a multiple shooting method similar to the one usually used for the numerical solution of boundary-value problems.[4] As in the standard procedure, we first split the total time span $[t_0, t_f]$ into a number of shorter subintervals selecting $m + 1$ equally spaced points $t_0, t_1, \ldots, t_m = t_f$. Moreover, for this particular implementation, all the epochs t_j, $j = 0, \ldots, m$, are considered fixed. We define $\mathbf{z}_j := \mathbf{z}(t_j)$, $j = 1, \ldots, m-1$, the state at the patch point j, obtained from the numerical integration in NCSEM coordinates of the solution of the Cauchy problem

$$\dot{\mathbf{z}} = \mathbf{f}(\mathbf{z}, t), \quad \mathbf{z}(t_0) = \boldsymbol{C}_e^s \circ \mathbf{W}_u(\mathbf{s}_0, \omega_s t_0). \tag{20}$$

Furthermore, the initial and final points $\mathbf{z}_0$ and $\mathbf{z}_m$ include the semi-analytical description of the initial and final sets:

$$\mathbf{z}_0(\mathbf{s}_0, t_0) = \boldsymbol{C}_e^s \circ \mathbf{W}_u(\mathbf{s}_0, \omega_s t_0), \quad \mathbf{z}_m(\mathbf{q}_f, t_m) = \mathbf{W}_s(\mathbf{q}_f, \omega_s t_m). \tag{21}$$

Let $\boldsymbol{\phi}(t_{j+1}, t_j; \mathbf{z}_j)$ be the image of the point $\mathbf{z}_j$ from t_j to t_{j+1} under the flow associated to the equations of motion (20). Since all epochs are fixed, all time spans are equal: $\Delta t := t_{j+1} - t_j = t_1 - t_0$. We then choose to discard the time dependency in the flow and denote $\boldsymbol{\phi}(\mathbf{z}_j) := \boldsymbol{\phi}(t_{j+1}, t_j; \mathbf{z}_j)$. Finally, the following vector of free variables is defined:

$$\mathbf{a} := \begin{pmatrix} \mathbf{s}_0^T & \mathbf{z}_1^T & \mathbf{z}_2^T & \cdots & \mathbf{z}_{m-1}^T & \mathbf{q}_f^T \end{pmatrix}^T. \tag{22}$$

Then, finding a continuous solution of the TPBVP (14) is equivalent to finding a zero of the following function $\mathbf{G}(\mathbf{a})$:

$$\mathbf{G}(\mathbf{a}) = \begin{pmatrix} \boldsymbol{\phi}(\mathbf{z}_0(\mathbf{s}_0, t_0)) \\ \boldsymbol{\phi}(\mathbf{z}_1) \\ \vdots \\ \boldsymbol{\phi}(\mathbf{z}_{m-1}) \end{pmatrix} - \begin{pmatrix} \mathbf{z}_1 \\ \mathbf{z}_2 \\ \vdots \\ \mathbf{z}_m(\mathbf{q}_f, t_m) \end{pmatrix} \tag{23}$$

In the general three-dimensional case, $\mathbf{G}$ has $6m + 3$ variables and $6m$ components, hence, contrary to the standard multiple shooting method, the associated system is not square. This is ought to the fact that there is no additional constraints on the initial and final states; instead, the latter are provided by the functions $\mathbf{z}_0(\mathbf{s}_0, t_0)$ and $\mathbf{z}_m(\mathbf{q}_f, t_m)$ that inherently contain the boundary conditions. This trick – and the semi-numerical procedures that underlies it – is what make the entire refinement procedure possible.

Given an initial guess $\mathbf{a}^0$ provided by the search algorithm, we can find the nearby zero $\mathbf{a}^*$ of $\mathbf{G}$ via a classic Newton-Raphson (NR) procedure. In our case, we also constantly check that the $\mathbf{s}_0$ and $\mathbf{q}_f$ stay in their respective domain of practical convergence.

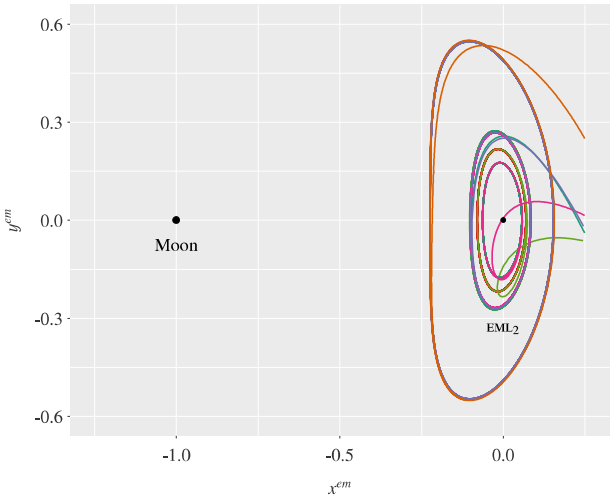

Fig. 6.: Focus on the lunar region in NCEM coordinates for the results of Figure 5, and with an identical color code. The lunar radius is not to scale.

5.1.1. Example of planar results

In order to apply the refinement procedure to planar connections, initial conditions $\mathbf{a}_0$ are taken in some families displayed on Figure 4. Each first guess is then refined using the multiple shooting method, yielding a final solution $\mathbf{a}^*$. The resulting orbits at both ends can then computed on an arbitrary time span – here equal to $10T$.

The corresponding results are displayed on Figure 5 in NCSEM coordinates, and on Figure 6 in NCEM coordinates, focused on the lunar region. Several types of connection appear among these solutions, with distinctive features such as the number of Earth flybys, or the number of visits of each libration regions. The solution on the upper left plot belongs to what is called here the *primary family*, which consists of direct transfers without any flyby or twist of the trajectory. Note that, given its unique simple structure, it is not difficult to isolate the primary family both in the projection and refinement procedures.

5.2. The continuation procedure in the planar case

The multiple shooting procedure allows to refine single EML$_2$-SEML$_{1,2}$ connections. As it has been seen on Figures 4 and 5, these connections are grouped in distinct one-parameter families – at least in the planar case and for a fixed initial time. From this observation, a continuation procedure based on ideas from the predictor-corrector methods[9] has been implemented. The result is a sequence of solutions $\mathbf{a}_p^*$, $p \in \mathbb{N}$, from which we can extract the initial conditions $x_{0,p}^{em,*}$ and $y_{0,p}^{em,*}$ at EML$_2$.

Each solution of Figure 5 has been continued using such algorithm. The results are visible on Figure 7. On the bottom center plot of this Figure are represented the starting points $(x_{0,p}^{em,*}, y_{0,p}^{em,*})$ at EML$_2$ of all the resulting transfers, superimposed with the results of Figures 4 and 5. One can see that, in all cases, the continued families match the valleys of solutions already detected via the projection map of Figure 4a, which validates the use of such maps as a preliminary detection tool. Moreover, as visible on Figure 7, it is possible to continue the family beyond the original scope of the projection map without any break down of the semi-analytical expansions, which is promising for the extension of such tool to bigger orbits.

All the procedures presented so far can be easily transposed to the EML$_2$-SEML$_1$ case, yielding quite similar results, with a quasi-symmetry with respect to the plane $t_0 = 0.5T$.

Moreover, they can be extended to the three-dimensional case by imposing constant non null values of the s_2 and s_4 components in the departure point at EML$_2$. With this choice, families of connections with a constant vertical extension at EML$_2$ are obtained. The resulting trajectories will be presented in a forthcoming paper, along with a more comprehensive work on the planar case.

6. Refinement of the primary family to JPL ephemerides

Enclosing the most direct natural transfers, the primary family is of fundamental importance for the understanding of the coupling between the libration regions of the SEM system. In order to test the relevance of the primary trajectories found in the QBCP, a refinement procedure to a higher-fidelity model is implemented, with the following key features:

- The non-relativistic gravitational influence of the Sun, the eight planets, the Moon and Pluto is taken into account in the higher-fidelity model. The position and velocity of the primaries involved are computed using the DE430 ephemerides from JPL.[12]
- A refined EML$_{1,2}$-SEML$_{1,2}$ QBCP connection is taken as initial guess, which provides initial conditions $(\mathbf{s}_i, t_i)$ inside $\mathbf{W}_u$ at EML$_{1,2}$, as well as final conditions $(\mathbf{q}_f, t_f)$ inside $\mathbf{W}_s$ at SEML$_{1,2}$. A complete three-legged connection trajectory is computed. It is composed of the transfer leg as well as the orbits at both ends, numerically integrated for a given number of periods of the SEM system. The resulting trajectory is discretized in patch points.
- A time correspondence is established with the higher-fidelity model by looking for the best fit between the Sun-Earth-Moon relative configuration at $t = t_i$ in the QBCP and the real positions of the primaries in the ephemerides. Once this correspondance is obtained, the patched point are transposed into an Earth-centered inertial frame associated to the ephemerides.
- To ensure the continuity of the trajectory, a multiple shooting procedure is implemented with free boundary conditions.[20]

A discrete set of trajectories has been selected within the primary family at $t_0 = 0.995T$ and successfully refined using this method. Figure 8 presents the results for four different primary solutions. Looking at Figure 8d, one can see that the sizes of the EML$_2$ orbits are mainly preserved after the refinement process, this assertion being however less and less true as the orbits grow. The same remark can be made on the SEML$_2$ final orbits on Figure 8a. Such trend is quite encouraging although it must be validated on other families.

7. Conclusion

A new approach is proposed for the systematic detection and refinement of SEML$_{1,2}$-EML$_{1,2}$ connections, based on a single dynamical model for the Sun-Earth-Moon (SEM) system: the Quasi-Bicircular Problem (QBCP), which is a periodic coherent

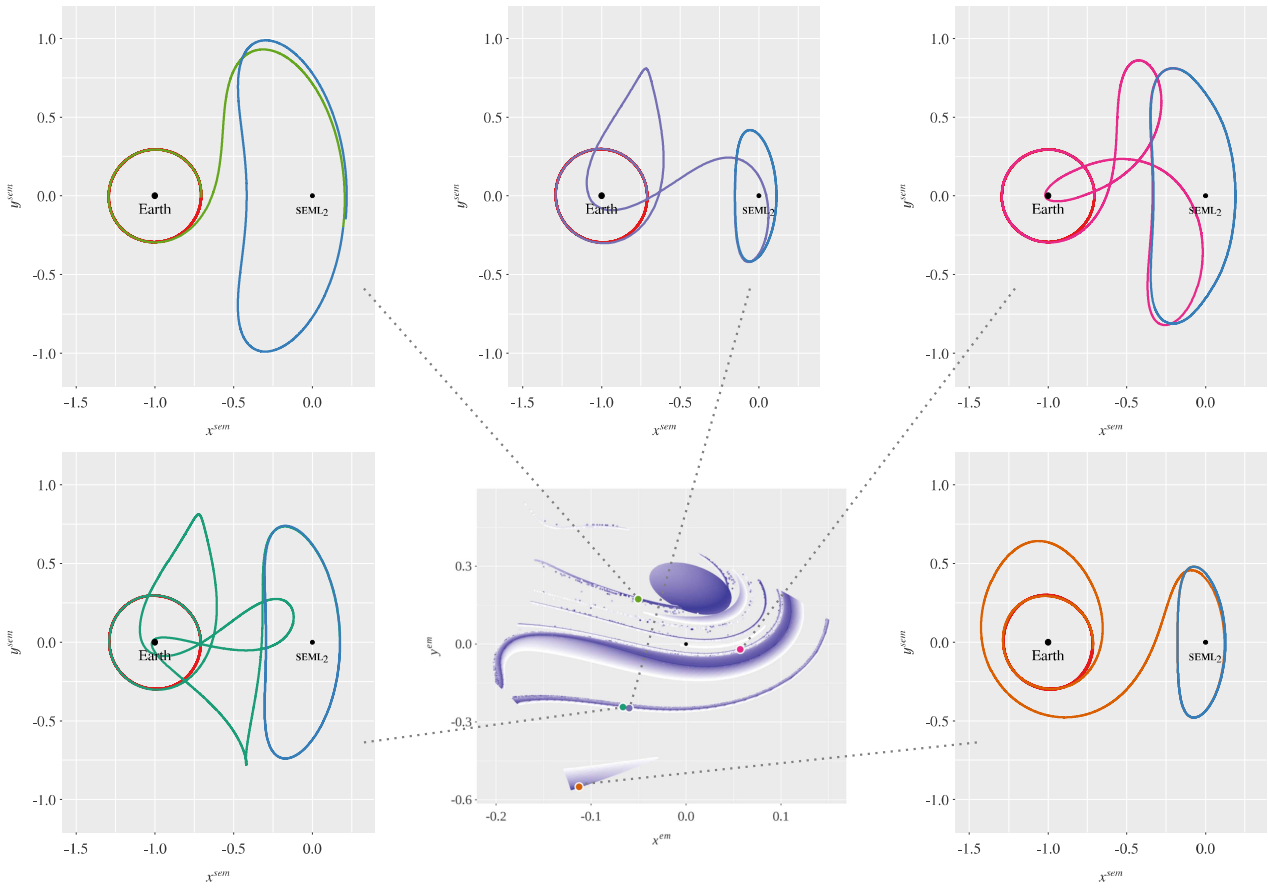

Fig. 5.: Some examples of planar EML$_2$-SEML$_2$ connections, refined from first guesses selected on Figure 4b, the latter being displayed again in the bottom center panel. On each solution, the orbit about EML$_2$ (resp. SEML$_2$) is plotted in bright red (resp. bright blue). The color of the transfer leg matches the dot that positions the corresponding starting point on the central (x^{em}, y^{em})-map, in NCEM coordinates. The trajectories are displayed in NCSEM coordinates.

approximation of the SEM motion. Although the gravitational influence of the three primaries is taken into account at all times, the perturbation associated to the third primary is small enough to preserve the key structures inherited from the separated dynamics of the Earth-Moon and Sun-(Earth+Moon) Circular Restricted Three-Body Problems (CRTBP).

Using an extension of the parameterization method, a semi-analytical description of the dynamics in the neighborhood of all four libration points has been obtained, including their center, center-stable and center-unstable manifolds. It has been shown that such objects can be used not only to compute initial conditions about a libration point but also to estimate the distance between any trajectory and the center manifold associated to another libration point – i.e. the set of all the staging orbits in its immediate vicinity. If this distance is close to zero, a connection between that trajectory and the targeted center manifold is expected to exist nearby. Using the semi-analytical parameterizations at both ends then allows to easily draw maps of possible connections – especially in the planar case for which the problem has been reduced to two-dimensional maps.

The refinement of the possible connections – first in the QBCP and then in a higher-fidelity model – validates the detection tool as an important step towards the systematic analysis of the dynamical couplings between the libration regions of the Earth-Moon and Sun-Earth systems.

Acknowledgments

The authors thank Denis Matignon and Alex Wittig for helpful discussions. This research has been supported by the AMX grant program of the École Polytechnique ParisTech. G.G. thanks the Catalan grant government for the grant 2014SGR1145, and MINECO-FEDER for the grants MTM2013-41168-P and MTM2016-80117-P. J.J.M. thanks MINECO-FEDER for the grant MTM2015-65715-P and the Catalan government for the grant 2014SGR504.

References

1) M. A. Andreu. *The Quasi-Bicircular Problem*. PhD thesis, Universitat de Barcelona, Spain, 1998.
2) M. A. Andreu. Dynamics in the center manifold around L$_2$ in the quasi-bicircular problem. *Celestial Mechanics and Dynamical Astronomy*, 84:105–133, 2002.
3) B. T. Barden, K. C. Howell, and M. W. Lo. Application of dynamical systems theory to trajectory design for a libration point mission. *Journal of the Astronautical Sciences*, 45(2):161–178, 1996.
4) R. Bulirsch and J. Stoer. *Introduction to numerical analysis*. Springer Heidelberg, 2002.
5) X. Cabré, E. Fontich, and R. De La Llave. The parameterization method for invariant manifolds I: Manifolds associated to non-resonant subspaces. *Indiana University Mathematics Journal*, 52(2):283–328, 2003.
6) E. Canalias. *Contributions to libration orbit mission design using*

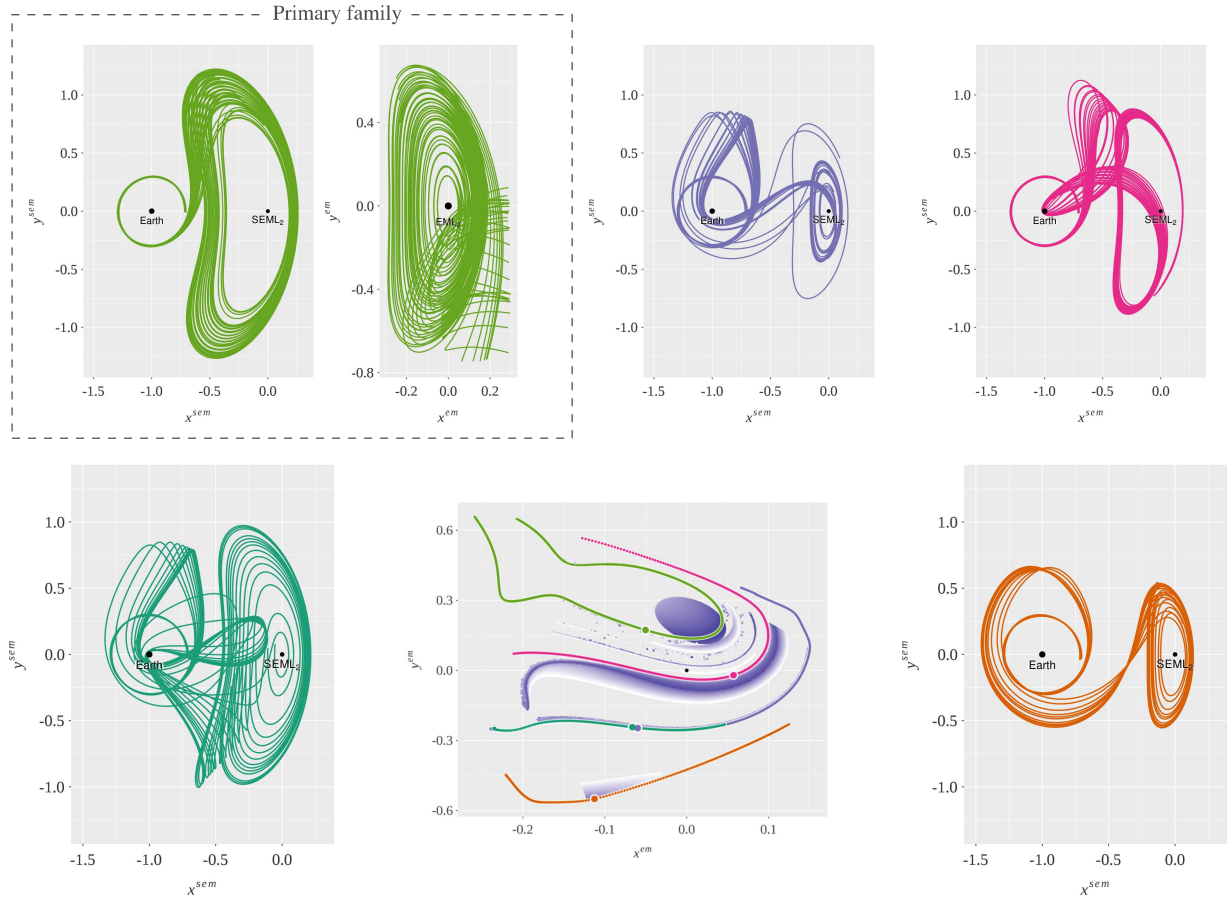

Fig. 7.: Continuation of the planar EML$_2$-SEML$_2$ connections from the results of Figure 5. The color of the transfer leg matches the one of the dots that position each starting point on the central (x^{em}, y^{em})-map, in NCEM coordinates. The trajectories are displayed in NCSEM coordinates, except for the primary family for which a focus at EML$_2$ in NCEM coordinates is also shown. Note that the initial and final orbits are not displayed.

hyperbolic invariant manifolds. PhD thesis, 2007.

7) E. Canalias and J. J. Masdemont. Computing natural transfers between Sun-Earth and Earth-Moon Lissajous libration point orbits. *Acta Astronautica*, 63(1-4):238–248, 2008.
8) E. Castella and À. Jorba. On the vertical families of two-dimensional tori near the triangular points of the bicircular problem. *Celestial Mechanics*, 76(1):35–54, 1999.
9) E. J. Doedel, D. J. Dichmann, J. Galán-Vioque, H. B. Keller, R. C. Paffenroth, and A. Vanderbauwhede. Elemental periodic orbits of the CR3BP: A brief selection of computational results. In *Equadiff 2003: International Conference On Differential Equations*, pages 163–168, 2003.
10) E. Fantino, G. Gómez, J. J. Masdemont, and Y. Ren. A note on libration point orbits, temporary capture and low-energy transfers. *Acta Astronautica*, 67(9):1038–1052, 2010.
11) N. Fenichel. Persistence and Smoothness of Invariant Manifolds for Flows. *Indiana Univ. Math. J.*, 21(3):193–226, 1972.
12) W. M. Folkner, J. G. Williams, D. H. Boggs, R. S. Park, and P. Kuchynka. The Planetary and Lunar Ephemerides DE430 and DE431. *Interplanet. Netw. Prog. Rep*, 196:42–196, 2014.
13) D. C. Folta, M. Woodard, K. C. Howell, C. E. Patterson, and W. Schlei. Applications of multi-body dynamical environments: The ARTEMIS transfer trajectory design. *Acta Astronautica*, 73:237–249, 2012.
14) F. Gabern and À. Jorba. A restricted four-body model for the dynamics near the Lagrangian points of the Sun-Jupiter system. *Discrete and Continuous Dynamical Systems series B*, 1(2):143–182, 2001.
15) G. Gómez, À. Jorba, J. J. Masdemont, and C. Simó. A dynamical systems approach for the analysis of the SOHO mission. In *Third International Symposium on Spacecraft Flight Dynamics, European Space Agency, Darmstadt, Germany*, pages 449–454, 1991.
16) G. Gómez, À. Jorba, J. J. Masdemont, and C. Simó. Dynamics and Mission Design Near Libration Points. Vol. IV. In *World Scientific Monograph Series*, volume 5. 2001.
17) G. Gómez, W. S. Koon, M. W. Lo, J. E. Marsden, J. J. Masdemont, and S. D. Ross. Invariant manifolds, the spatial three-body problem and space mission design. In D. B. Spencer, C. C. Seybold, A. K. Misra, and R. J. Lisowski, editors, *Advances in the Astronautical Sciences*, volume 109, pages 3–22. American Astronautical Society, San Diego, 2001.
18) G. Gómez, W. S. Koon, M. W. Lo, J. E. Marsden, J. J. Masdemont, and S. D. Ross. Connecting orbits and invariant manifolds in the spatial restricted three-body problem. *Nonlinearity*, 17(5):1571–1606, 2004.
19) G. Gómez, J. Llibre, R. Martínez, and C. Simó. Dynamics and mission design near libration points. Vol I. In R. Donagi, R. de la Llave, and M. Shubin, editors, *World Scientific Monograph Series*, volume 2. World Scientific, 2001.
20) G. Gómez, J. J. Masdemont, and C. Simó. Quasihalo orbits associated with libration points. *Journal of the Astronautical Sciences*, 46(2):135–176, 1998.
21) À. Haro, M. Canadell, J. L. Figueras, A. Luque, and J. M. Mondelo. *The parameterization method for invariant manifolds: from rigorous results to effective computations*, volume 195. Springer, 2016.
22) K. C. Howell and M. Kakoi. Transfers between the Earth-Moon and Sun-Earth systems using manifolds and transit orbits. *Acta Astronautica*, 59(1-5):367–380, 2006.
23) À. Jorba. A methodology for the numerical computation of normal forms, centre manifolds and first integrals of Hamiltonian systems. *Experimental Mathematics*, 8(2):155–195, 1999.
24) À. Jorba and J. J. Masdemont. Dynamics in the center manifold of

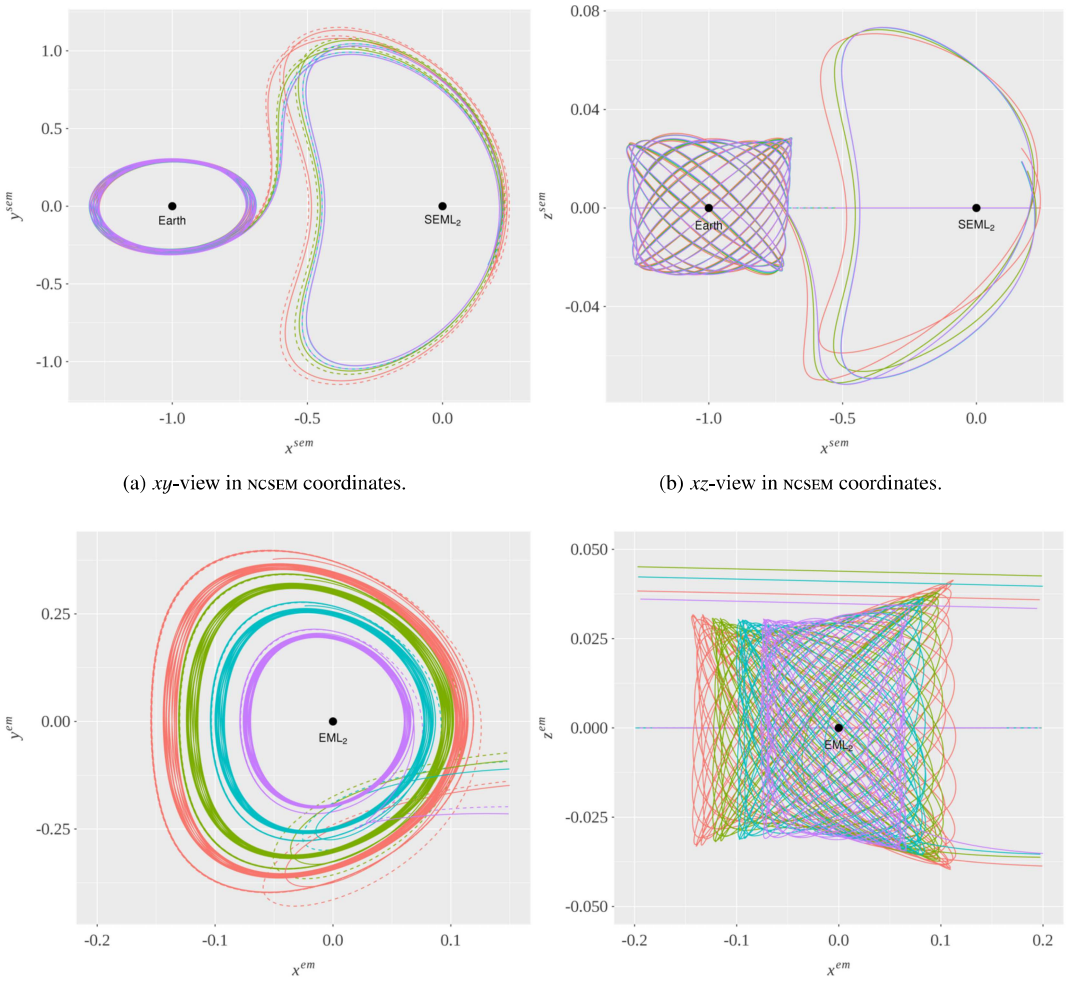

(a) *xy*-view in NCSEM coordinates.

(b) *xz*-view in NCSEM coordinates.

(c) Zoom at EML_2, in NCEM coordinates.

(d) Zoom at EML_2, in NCEM coordinates.

Fig. 8.: Example of four different refinements to JPL ephemerides. Each solution as a distinctive color. The initial (planar) QBCP trajectories are dotted, while the final trajectories are given in solid lines. Note that the plot aspect ratio is not equal to one in any of the figures.

the collinear points of the restricted three body problem. *Physica D: Nonlinear Phenomena*, 132(1):189–213, 1999.

25) W. S. Koon, M. W. Lo, J. E. Marsden, and S. D. Ross. Shoot the moon. In *AAS/AIAASpace Flight Mechanics Meeting*, pages 1017–1030, 2000.

26) W. S. Koon, M. W. Lo, J. E. Marsden, and S. D. Ross. Low energy transfer to the Moon. In *Dynamics of Natural and Artificial Celestial Bodies*, pages 63–73. Springer, 2001.

27) B. Le Bihan, J. J. Masdemont, G. Gómez, and S. Lizy-Destrez. Dynamics in the center manifold around equilibrium points in periodically perturbed three-body problems. In *International Conference on Astrodynamics Tools and Techniques*, Darmstadt, Germany, 2016.

28) B. Le Bihan, J. J. Masdemont, G. Gómez, and S. Lizy-Destrez. Invariant manifolds of a non-autonomous quasi-bicircular problem computed via the parameterization method. *Preprint*, 2017.

29) L. Lindegren, C. Babusiaux, C. Bailer-Jones, U. Bastian, A. G. A. Brown, M. Cropper, E. Høg, and Others. The Gaia mission: science, organization and present status. In *International Astronomical Union, IAU Symposium*, volume 248, pages 217–223, 2008.

30) J. J. Masdemont. High-order expansions of invariant manifolds of libration point orbits with applications to mission design. *Dynamical Systems: An International Journal*, 20(1):59–113, 2005.

31) J. S. Parker. Families of low-energy lunar halo transfers. In *AAS/AIAA Spaceflight Dynamics Conference*, volume 90, pages 1–20, 2006.

32) D. L. Richardson. Analytic construction of periodic orbits about the collinear points. *Celestial mechanics*, 22(3):241–253, 1980.

33) C. Roberts, S. Case, J. Reagoso, and C. Webster. Early Mission Maneuver Operations for the Deep Space Climate Observatory Sun-Earth L1 Libration Point Mission. In *AIAA/AAS Astrodynamics Specialist Conference*, number 595, pages 1–21, 2015.

34) V. Szebehely. Theory of orbits: the restricted problem of three bodies. Technical Report 3, DTIC Document, 1967.

35) F. Topputo. On optimal two-impulse Earth-Moon transfers in a four-body model. *Celestial Mechanics and Dynamical Astronomy*, 117(3):279–313, 2013.

36) K. Yagasaki. Sun-perturbed earth-to-moon transfers with low energy and moderate flight time. *Celestial Mechanics and Dynamical Astronomy*, 90(3-4):197–212, 2004.

37) A. Zanzottera, G. Mingotti, R. Castelli, and M. Dellnitz. Intersecting invariant manifolds in spatial restricted three-body problems: Design and optimization of Earth-to-halo transfers in the Sun-Earth-Moon scenario. *Communications in Nonlinear Science and Numerical Simulation*, 17(2):832–843, 2012.